Gurnis, M. E. Wysession, E. Knittle, B. A. Buffett, Eds. (American Geophysical Union, Washington, DC, in press).
13. J. Mori and D. V. Helmberger, *J. Geophys. Res.* **100**, 20359 (1995).
14. In constructing Fig. 1, we incorporated only those ray paths for which anomalous diffracted *P*-wave segments of the seismic phase *SPdKS* could be resolved to lie on either the source or receiver side of the ray path, as derived from different paths containing overlapping diffracted segments (*9*, *12*). The lateral extent of ULVZs was determined by standard Fresnel zone analysis (*19*) including all regions sampled within the first quarter period. Varying the assumed size of the Fresnel zone affected our statistical correlations, with smaller and larger zones producing somewhat worse correlations between hot spots and the ULVZs. Nevertheless, ULVZs are better correlated with hot spot flux than any contours within tomographic velocity models of the deep mantle (*4*, *19*) for Fresnel zone dimensions between one-eighth and one-half wavelength.
15. N. M. Ribe and D. P. de Valpine, *Geophys. Res. Lett.* **21**, 1507 (1994).
16. T. W. Ray and D. L. Anderson, *J. Geophys. Res.* **99**, 9605 (1994).
17. S. T. Crough, *Tectonophysics* **61**, 321 (1979).
18. Our results are not particularly sensitive to our areal sampling size around hot spots; distances from 0.5° to 4° produce similar statistical correlations.
19. M. E. Wysession, *Nature* **382**, 244 (1996).
20. Those hot spots that lie above regions where ULVZs have not been observed could be (i) associated with highly localized (and as yet undetected) ULVZs, (ii) produced by lateral flow or deflection of plumes (*22*), or (iii) derived from a different depth or through a different process than ULVZ-associated hot spots.
21. C. G. Chase and D. R. Sprowl, *Earth Planet. Sci. Lett.* **62**, 314 (1983).
22. N. H. Sleep, *J. Geophys. Res.* **97**, 20007 (1992).
23. W. J. Morgan, *ibid.* **83**, 5355 (1978); N. H. Sleep, *ibid.* **101**, 28065 (1996).
24. P. Olson and I. S. Nam, *ibid.* **91**, 7181 (1986).
25. W. J. Morgan, *Tectonophysics* **94**, 123 (1983); B. C. Storey, *Nature* **377**, 301 (1995).
26. W. J. Morgan, *Geol. Soc. Am. Mem.* **132**, 7 (1972); R. E. Sheridan, *Tectonophysics* **143**, 59 (1987); M. A. Richards, R. A. Duncan, V. E. Courtillot, *Science* **246**, 103 (1989); I. H. Campbell and R. W. Griffiths, *Earth Planet. Sci. Lett.* **99**, 79 (1990).
27. T. Lay, Q. Williams, E. J. Garnero, *Nature* **392**, 461 (1998).
28. K. M. Fischer *et al.*, *Eos* **77**, F678 (1996).
29. Standardized score (z) is defined as $z = (O - E)/\sigma$, where O is the number of hot spots (or flux) inside a velocity contour for a randomly sampled 44% of the tomographic models, E denotes the number (or flux) predicted by a binomial distribution, and σ is the standard deviation of the binomial. Zero corresponds to uncorrelated data; $z \geq 1.0$ has an ~15% likelihood of arising randomly.
30. Supported by the NSF Geophysics and Presidential Faculty Fellow programs. We thank H. Nataf and the reviewers for comments on the manuscript.

20 March 1998; accepted 21 May 1998

Fast Recession of a West Antarctic Glacier

E. J. Rignot

Satellite radar interferometry observations of Pine Island Glacier, West Antarctica, reveal that the glacier hinge-line position retreated 1.2 ± 0.3 kilometers per year between 1992 and 1996, which in turn implies that the ice thinned by 3.5 ± 0.9 meters per year. The fast recession of Pine Island Glacier, predicted to be a possible trigger for the disintegration of the West Antarctic Ice Sheet, is attributed to enhanced basal melting of the glacier floating tongue by warm ocean waters.

Pine Island Glacier is a major ice stream of West Antarctica (*1*–*7*) that has been highlighted as being vulnerable to climate change and a possible trigger for the disintegration of the West Antarctic Ice Sheet (*6*, *7*). The ice stream flows rapidly into Pine Island Bay, in the Amundsen Sea, unrestrained by a large ice shelf at its junction with the ocean, over a subglacial bed well below sea level, which deepens inland. This flow configuration is theoretically unstable (*8*, *9*) because a retreat of its grounding line (where the glacier reaches the ocean and becomes afloat) would be self-perpetuating and irreversible, regardless of climate forcing.

Early estimates of the ice-stream mass budget suggested that it was thickening (*3*, *4*). The result was called into question (*5*), but not enough reliable data existed on the ice flow and grounding line to allow a precise mass balance calculation. More recently, a hydrographic survey of Pine Island Bay revealed that the glacier experiences basal melt rates one order of magnitude larger than those recorded on large Antarctic ice shelves (*10*, *11*). High basal melting is apparently fueled by an influx of relatively warm ocean waters from the southern Pacific Ocean (*10*). Such basal melting brings new considerations for the mass budget of the glacier floating section (*1*).

Here, I applied a quadruple difference interferometry technique (*12*, *13*) on radar data gathered by the Earth Remote Sensing instruments (ERS-1 and -2) to detect the hinge-line position (or limit of tidal flexing) across Pine Island Glacier and its migration with time (*14*) (Fig. 1). Feature tracking based on the phase correlation method was used with the same data to yield detailed vector measurements of the glacier velocity on both grounded and floating ice (*15*). The glacier surface elevation was obtained from a new digital elevation model (DEM) of Antarctica (*16*).

Combining the glacier hinge-line position, velocity, and surface elevation, I calculated that the ice discharge is 76 ± 2 km^3 of ice year^{-1} at the hinge line (*17*). The estimated mass input from interior regions is 71 ± 7 km^3 of ice year^{-1} (*18*). These numbers suggest a mass deficit of 5 ± 7 km^3 of ice year^{-1} upstream of the hinge line (*19*).

The hinge-line positions retrieved in 1992, 1994, and 1996 (*20*) indicate a hinge-line retreat at a mean rate of 1.2 ± 0.3 km year^{-1} (Fig. 1, B to F, and Fig. 2, A and B). Hinge-line retreat may result from an increase in sea-level height or a decrease in ice thickness (a decrease in the height of the seabed causes retreat too, but the effect is insubstantial over the time scale considered here) (*7*–*9*). Changes in sea level due to ocean tide yield an uncertainty in hinge-line position of less than 1.3 km per interferogram and 0.3 km year^{-1} in mean retreat rate (*21*). I therefore attribute the 1992 to 1996 retreat to a decrease in ice thickness. The calculated *rate of thinning is 3.5 ± 0.9 m of ice year*$^{-1}$ at the hinge line.

Mass accumulation [+0.4 m year^{-1} in (*1*)] and sublimation [−0.7 m year^{-1} in (*22*)] at the glacier surface are too small to cause a major change in the glacier surface budget. A more likely explanation for the thinning is that the bottom melt rates experienced by the glacier have been too large to maintain the floating tongue in a state of mass balance (*23*).

Calculations of ice discharge seaward of the hinge line indicate that basal melting has exceeded 50 ± 10 m year^{-1} in the first 20 km of the subice cavity, decreasing to an average of 24 ± 4 m year^{-1} between the hinge line and the calving front (Fig. 2C). The large melt rates recorded near the hinge line imply that Pine Island Glacier is even more sensitive to ice-ocean interactions than was inferred from the 1994 survey of ice-front conditions (*10*).

Application of a two-dimensional thermohaline circulation model to the subice cavity reveals how sensitive basal melting is to changes in ocean conditions. An increase in seawater temperature from +1.5° to +2.0°C increases basal melting by 30% (*11*). A 3.5–m year^{-1} thinning could therefore result from a one-tenth of a degree Celsius increase in seawater temperature, which is not unlikely for the deep water in

Jet Propulsion Laboratory, California Institute of Technology, MS 300-235, Pasadena, CA 91109–8099, USA. E-mail: eric@adelie.jpl.nasa.gov

the southeast Pacific (*24*).

Sediment cores collected in Pine Island Bay show that a substantially more extensive ice-shelf cover was present perhaps as recently as 100 years ago in Pine Island Bay (*25*). Terminus locations recorded in 1966, 1973, and 1985 indicated an ice-front retreat of 0.8 km year^{-1}. More recent satellite imagery, however, suggested that the ice front has been stable (*1*, *5*).

The ice-front evolution is probably controlled by physical processes that operate on a different time scale than those driving hinge-line retreat. Basal melting is low at the ice front (Fig. 2C) and less prone to induce thinning. The ice-front position is pinned down by numerous emerging islands or ice rises (Fig. 1A) that may temporarily slow or halt its retreat. The periodic calving of massive icebergs (Fig. 1A) complicates the analysis of ice-front migration over short time scales. In contrast, rapid melting near the hinge line has an immediate effect on the hinge-line position because that position is governed by hydrostatic equilibrium of the ice.

Whether the retreat of Pine Island Glacier is a unique, short-lived phenomenon or the signal of a wider scale, longer term ice-sheet disintegration cannot be answered at present. If basal melting does drive the retreat, however, other ice-sheet sectors of the Amundsen and Bellingshausen seas where the continental shelf is invaded by warm circumpolar deep water (*1*, *11*) could be retreating.

References and Notes

1. A. Jenkins, D. G. Vaughan, S. S. Jacobs, H. H. Hellmer, J. R. Keys, *J. Glaciol.* **43**, 114 (1997).
2. D. Lindstrom and D. Tyler, *Antarct. J. U.S.* **19**, 53 (1984).
3. D. Lindstrom and T. J. Hughes, *ibid.*, p. 56.
4. R. D. Crabtree and C. S. M. Doake, *Ann. Glaciol.* **3**, 65 (1982).
5. B. K. Lucchitta, C. E. Rosanova, K. F. Mullins, *ibid.* **21**, 277 (1995).
6. T. J. Hughes, *J. Glaciol.* **24**, 493 (1979); *ibid.* **27**, 518 (1981); G. H. Denton *et al.*, *ibid.* **24**, 495 (1979); C. S. Lingle and J. A. Clarke, *ibid.*, p. 213; R. H. Thomas, *ibid.*, p. 167.
7. M. Stuiver, G. H. Denton, T. J. Hughes, J. L. Fastook, in *The Last Great Ice Sheets*, G. H. Denton and T. J. Hughes, Eds. (Wiley, New York, 1981), pp. 319–346.
8. J. Weertman, *J. Glaciol.* **13**, 3 (1974); R. H. Thomas and C. R. Bentley, *Quat. Res.* **10**, 150 (1978); R. H. Thomas, T. J. O. Sanderson, K. E. Rose, *Nature* **277**, 355 (1979).
9. R. H. Thomas, in *Climate Processes and Climate Sensitivity*, J. E. Hansen and T. Takahashi, Eds., vol. 29 of Geophysical Monograph Series, vol. 5 of Maurice Ewing Series (American Geophysical Union, Washington, DC, 1984), pp. 265–274.
10. S. S. Jacobs, H. H. Hellmer, A. Jenkins, *Geophys. Res. Lett.* **23**, 957 (1996).
11. H. H. Hellmer, S. S. Jacobs, A. Jenkins, in *Antarctic Research Series*, vol. 75 (American Geophysical Union, Washington, DC, in press).
12. E. Rignot, *J. Glaciol.* **42**, 476 (1996); ———, S. P. Gogineni, W. B. Krabill, S. Ekholm, *Science* **276**, 934 (1997); E. Rignot, *Ann. Glaciol*, in press; *J. Glaciol.*, in press.
13. To locate a glacier hinge line with ERS radar interferometry, I formed the difference between two radar interferograms generated with data acquired 1 day apart (1996), 3 days apart (1994), and 6 days apart (1992). Differencing eliminates information common to both interferograms, which is the steady and continuous creep deformation of the glacier, a mostly horizontal motion. After differencing of the two interferograms, I removed the interferometric signal associated with the glacier topography given by an altimetric DEM of Antarctica (*16*) at a 5-km spacing, interpolated to the 20-m spacing of the radar interferograms. The coarse spatial resolution of the DEM is sufficient to remove the mean glacier surface slope (less than 2%) from the data. The resulting "quadruple" difference interferogram measures the glacier surface displacement along the radar line of sight (23° off vertical) in response to changes in ocean tide, which is a vertical motion. To process the 1992 and 1994 quadruple difference interferograms successfully, I first registered the radar scenes with subpixel precision (*15*) to follow the glacier motion (which exceeds 20 m in 3 days) and then generated radar interferograms at the finest spatial resolution before differencing.
14. The hinge line, or limit of tidal flexing, detected with radar interferometry is a surface proxy for the grounding line. The hinge-line position is mapped automatically by fitting (in the least squares sense) an elastic beam model of tidal flexure (*12*) through individual tidal displacement profiles extracted from difference interferograms across the zone of tidal flexure, in a direction perpendicular to the iso-contours of vertical displacement of the glacier. The mapping precision is highest (80 m) in areas of high signal-to-noise ratio, large tidal motion, and large radius of curvature of the hinge line; it degrades along the glacier side margins where the signal is limited by the resolution of the ERS radar imaging system. On average, the mapping precision is better than ±200 m.

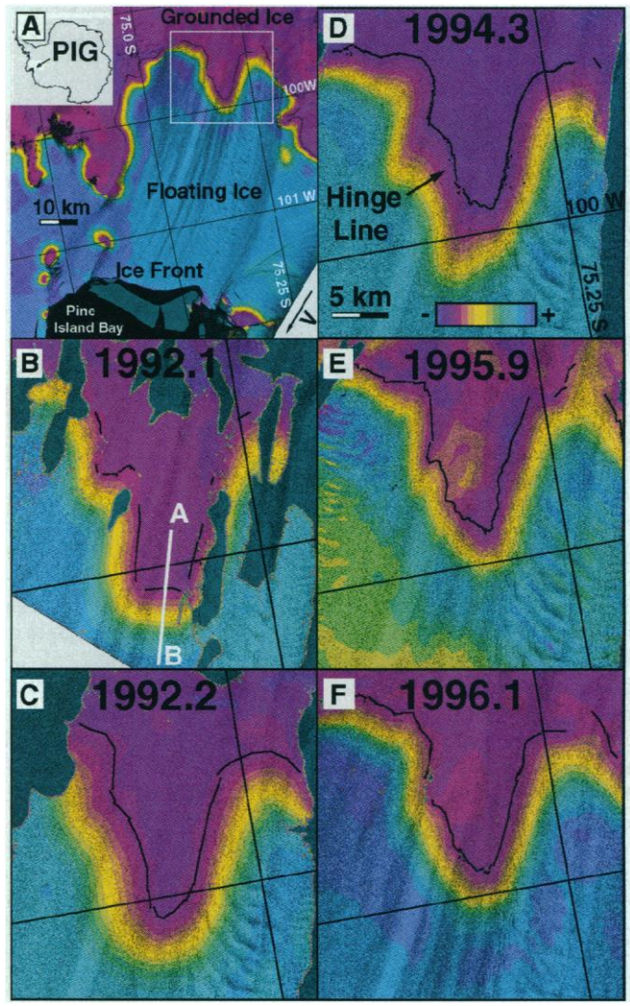

Fig. 1. Normalized tidal displacements of Pine Island Glacier (PIG), West Antarctica, recorded with ERS differential interferometry and color coded [color bar in (D)] from magenta (grounded ice) to yellow (glacier flexure zone) and blue (ice-shelf ice in hydrostatic equilibrium with the ocean waters). Color tone is modulated by the radar brightness of the scene acquired by ERS-1 on 21 January 1996 (orbit 23,627, frames 5589 and 5607). The glacier fast moving portion is revealed by flow-line features conspicuous in the radar brightness image. No interferometric data are available in areas colored dark green. The white square in (**A**) delineates the area shown in (**B**) to (**F**). ERS is flying north in (A), (B), and (F) (ascending track, heading −49° from N) and south in (C), (D), and (E) (descending track, heading −128° from N), illuminating the scene from its right. The tide normalization factors from (B) to (F) are 2.2, 4.0, 3.2, 2.7, and 0.9 m, respectively. The hinge-line position, retrieved from model fitting (*14*), is shown as a black, thin, continuous line separating grounded (magenta, minus sign) from floating ice (blue, positive sign). Its finger-shaped appearance in (B) to (F) indicates the presence of thicker ice at the glacier center than along its sides. In (A), locally grounded areas or ice rises appear in magenta between the hinge line and the ice front, in areas where the ice shelf is virtually stagnant. Profile A-B [thick, white line in (B)] is discussed in Fig. 2A. Hinge-line position and tidal displacements were recorded in (B) January 1992 (ERS-1 orbits 2970, 3056, and 3142; frame 5589), (C) February 1992 (ERS-1 orbits 3260, 3346, and 3432; frame 5211), (D) March 1994 (ERS-1 orbits 13,826, 13,869, and 13,912; frame 5211), (E) November 1995 and January 1996 (ERS-1/2 orbit pairs 22,614/2941 and 23,616/3943; frame 5211), and (F) January and February 1996 (ERS-1/2 orbit pairs 23,627/3954 and 24,128/4455; frame 5589). Between (B) and (F), the hinge line retreated 5.0 ± 1.0 km in 3.78 years over a 275-m-wide region at the glacier center. The retreat is less along the side margins presumably because of steeper slopes (−1.2% instead of −0.5% at the glacier center) and possibly less thinning (*21*).

15. ERS interferometry only measures the velocity of ice along the radar line of sight, which is a one-dimensional measurement. A combination of interferograms obtained along ascending and descending tracks could yield vector measurements of the glacier displacement, but this approach does not work on floating ice because the interferometric signal is contaminated by tidal motion. Instead, I used a novel feature-tracking technique based on the phase correlation method [R. Michel, thesis, Université Paris XI, Paris (1997)] that provides along- and across-track velocities at every point on a regular grid (spacing is 500 m), from the same image data. The along-track displacements are independent of tide and have a precision of 49 m year^{-1} for the 1-day pairs and 8 m year^{-1} for the 6-day pairs. The across-track displacements are five times less precise (spatial resolution is 20 m across track compared with 4 m along track) and affected by tide (3 m of tide compared with 13 m of creep flow in 6 days along the radar line of sight). Two independent estimates of the glacier motion were obtained for the 1992 and 1994 data to increase the measurement precision. The 1996 ice fluxes were calculated with only the along-track displacements with cross-glacier profiles oriented in the across-track direction.
16. J. Bamber and R. A. Bindschadler, *Ann. Glaciol.* **25**, 439 (1998).
17. Ice discharge through a cross-glacier profile is calculated as the discrete sum (50 to 60 points per profile) of the ice velocity normal to the profile multiplied by ice thickness along the profile. Ice thickness is deduced from the DEM with the assumption of hydrostatic equilibrium of the ice, a seawater density ρ_w = 1027.5 kg m^{-3} (*10*), and a depth-averaged density of ice ρ_i = 900 kg m^{-3} (*1*). Ice discharge calculated with the 1992, 1994, and 1996 data is 76.3, 75.1, and 77.1 km^3 of ice year^{-1}, respectively, at the hinge line. The mean discharge is 76.1 km^3 of ice year^{-1}. The precision is 2 km^3 of ice year^{-1} based on a ±30-m uncertainty in ice thickness.
18. A revised map of mass accumulation has been assembled on a 100-km grid (M. B. Giovinetto, personal communication). The drainage basin of Pine Island Glacier was drawn on the computer with a DEM (*16*) interpolated to a 1-km sample spacing, starting at low elevation from the precise end points of the profile selected for calculation of ice discharge at the hinge line. The resulting accumulation area is 159,000 ± 1000 km^2. Mass accumulation is 65.0 ± 7 km^3 year^{-1} w.e. (water equivalent), or 70.8 ± 7 km^3 of ice year^{-1} with ρ_i = 0.917 kg m^{-3}. Mass accumulation is known with 10% confidence in this region. Lindstrom and Hughes (*3*) estimated 65.9 km^3 year^{-1} w.e. accumulation, which is close to my estimate obtained from more accurate elevation data.
19. Earlier analyses (*3, 4*) suggested a large, positive mass budget based on underestimates of ice velocity at the grounding line (*5*). Lucchitta *et al.* (*5*) estimated a glacier discharge of 70 gigatons year^{-1} (76 km^3 year^{-1}) at a grounding-line position misplaced by Crabtree and Doake (*4*) 30 km upstream of my inferred grounding line. Jenkins *et al.* (*1*) estimated ice discharge at 56 gigatons year^{-1} at a location 12 km upstream of my inferred hinge line but using ice thickness data of uncertain positional accuracy (*1*). My analysis uses complete cross-glacier profiles of thickness and velocity at the precise location of the grounding line.
20. Multiyear ERS data from ascending and descending tracks were registered independently to reference scenes acquired in 1996 (ERS-1 orbit 23,627 for ascending tracks and ERS-1 orbit 23,616 for descending tracks) with the cross-correlation of the signal intensity over nonmoving parts of the scene. The precision of registration is better than ±40 m in the along- and across-track directions. Topographic information was required to register ascending and descending tracks together. I projected all data onto a common polar stereographic grid at 50-m spacing using surface elevation from the altimetric DEM of Antarctica. The two geocoded reference scenes for ascending and descending tracks (which were acquired 1 day apart) were subsequently coregistered to within ±50 m with the cross-correlation of the signal intensity over the entire area (glacial motion is less than 7 m in 1 day). This final coregistration provides the framework for comparing ascending and descending data of any year with ±60 m, which is two orders of magnitude less than the detected hinge-line migration.
21. Hinge-line positions migrate back and forth with time by $\dot{x}$ following changes in ocean tide $\dot{z}$ and ice thickness $\dot{h}$ according to

$$\dot{h} = (\rho_w/\rho_i)\dot{z} - [\alpha - \beta(1 - \rho_w/\rho_i)]\dot{x} \quad (1)$$

where $\dot{h} > 0$ for thickening, $\dot{x} > 0$ for hinge-line retreat, and α and β are the surface and basal slopes, respectively, counted positive upward (*7*). I estimate $\alpha = -0.5\%$ from the DEM (*16*) and $\beta = +1.1\%$ from the approximate grounding-line position proposed in (*9*) on the basis of the British Antarctic Survey thickness data collected in 1981 (*4*). β is uncertain, but its value has 10 times less influence than α in eq. 1. Hinge-line migration due to tide only is $\dot{x} = 332\dot{z}$. Ocean tides are unknown in Pine Island Bay, but the range of tides is constrained by the ERS observation of differential tide, which does not exceed 4 m (Fig. 1). Hinge-line migration due to tide should therefore not exceed 1.3 km. The corresponding uncertainty in hinge-line retreat rate for my five observations is 0.3 km year^{-1}. Hinge-line migration due to changes in ice thickness only is $\dot{x} = -290.6\dot{h}$. The 1.2 ± 0.3 km year^{-1} hinge-line retreat therefore translates into a thinning of $\dot{h}$ = 3.5 ± 0.9 m of ice year^{-1}.
22. T. B. Kellog, D. E. Kellog, T. J. Hughes, *Antarct. J. U.S.* **20**, 79 (1985).
23. Increased basal melting should increase the glacier velocity to compensate for mass loss and back pressure reduction from the floating tongue. The ice-front velocity of Pine Island Glacier has remained stable at the 10% level since the 1970s (*1*). I found no change in ice velocity between 1992 and 1996 at the 1% level. Hence, the grounding line was probably already retreating at the earliest times of observation.
24. J. H. Swift, *Int. WOCE Newsl.* **18**, 15 (1995).
25. T. B. Kellog and D. E. Kellog, *J. Geophys. Res.* **92**, 8859 (1987).

26. I thank the European Space Agency for providing ERS data; S. Jacobs, A. Jenkins, H. Hellmer, and D. Vaughan for discussions; J. Bamber for providing a DEM of Antarctica; G. Peltzer, P. Rosen, and three anonymous reviewers for comments; and M. Schmeltz, G. Buscarlet, and C. Werner for assistance. This work was carried out at the Jet Propulsion Laboratory, California Institute of Technology, under a contract with the Polar Program of NASA.

7 April 1998; accepted 11 June 1998

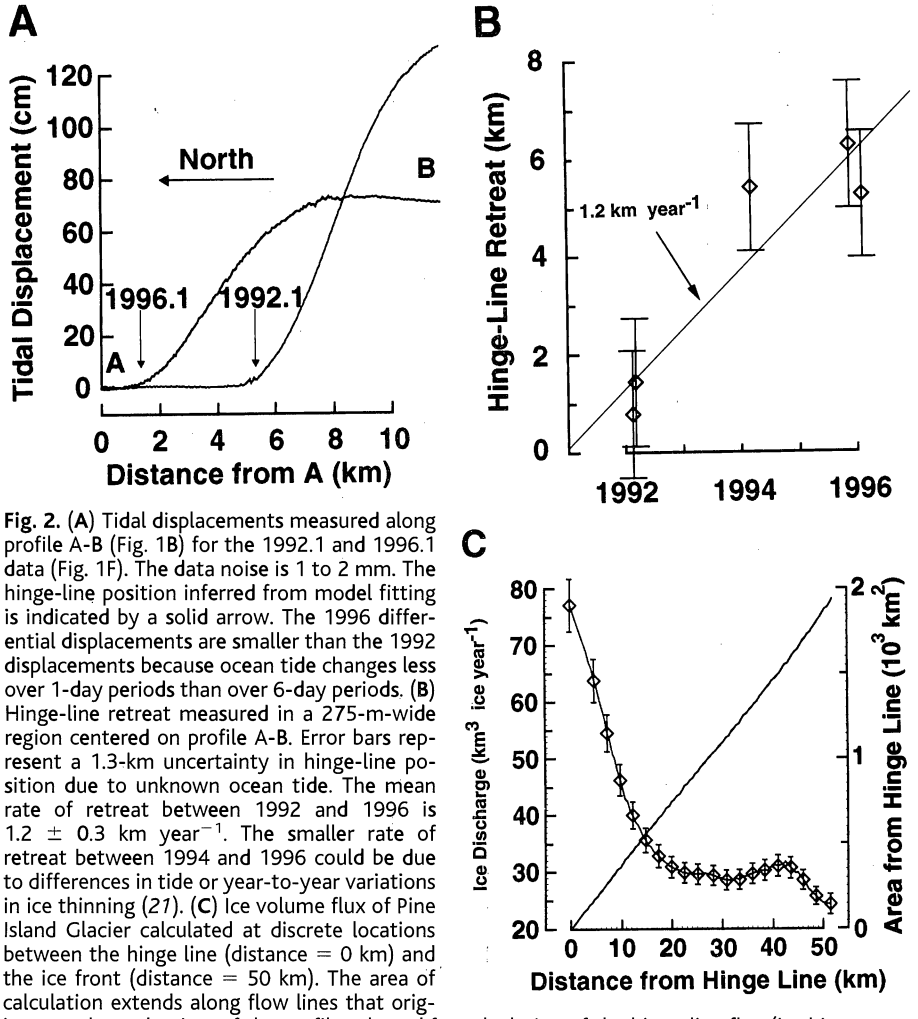

Fig. 2. (**A**) Tidal displacements measured along profile A-B (Fig. 1B) for the 1992.1 and 1996.1 data (Fig. 1F). The data noise is 1 to 2 mm. The hinge-line position inferred from model fitting is indicated by a solid arrow. The 1996 differential displacements are smaller than the 1992 displacements because ocean tide changes less over 1-day periods than over 6-day periods. (**B**) Hinge-line retreat measured in a 275-m-wide region centered on profile A-B. Error bars represent a 1.3-km uncertainty in hinge-line position due to unknown ocean tide. The mean rate of retreat between 1992 and 1996 is 1.2 ± 0.3 km year^{-1}. The smaller rate of retreat between 1994 and 1996 could be due to differences in tide or year-to-year variations in ice thinning (*21*). (**C**) Ice volume flux of Pine Island Glacier calculated at discrete locations between the hinge line (distance = 0 km) and the ice front (distance = 50 km). The area of calculation extends along flow lines that originate at the end points of the profile selected for calculation of the hinge-line flux (in this manner, the effect of ice-shelf spreading is taken into account). Conservation of mass within that area dictates that the steady-state rate of basal melting (calculated as the decrease in ice flux divided by the area) exceeds 50 m year^{-1} in the first 20 km and subsequently decreases toward the ice front. If the glacier is not in steady state and thins at 3.5 m year^{-1}, basal melting is effectively 53.5 m year^{-1}.